Hindawi
Shock and Vibration
Volume 2021, Article ID 6634086, 17 pages
https://doi.org/10.1155/2021/6634086

Research Article

Performance Assessment of Shockwaves of Chute Spillways in Large Dams

S. M. Mousavimehr, Omid Aminoroayaie Yamini, and M. R. Kavianpour

Department of Civil Engineering, K. N. Toosi University of Technology, Tehran, Iran

Correspondence should be addressed to Omid Aminoroayaie Yamini; o.aminoroaya@mail.kntu.ac.ir

Received 21 October 2020; Revised 17 November 2020; Accepted 15 January 2021; Published 20 February 2021

Academic Editor: Xiaowei Deng

Copyright © 2021 S. M. Mousavimehr et al. This is an open access article distributed under the Creative Commons Attribution License, which permits unrestricted use, distribution, and reproduction in any medium, provided the original work is properly cited.

Spillways are the most important structures of large dams that are responsible for releasing the excessive flood discharge from the reservoir. Although many studies have been performed to determine the flow characteristics over these structures, however, the available information on the shockwaves' characteristics for spillways' design is limited. The supercritical flow below the chute piers generates an aerated flow known as shockwaves. Due to the flow interaction with the chute piers, three kinds of standing waves just downstream of the pier, in the middle of the chute, and on the sidewalls are generated. This phenomenon affects the flow domain and its hydraulic characteristics along the chute spillway. The height of the waves increases downstream, where they hit the chute walls and reflect again into the flow to interact together again. The process repeated and intensified downstream in a lozenge shape. The height of these waves can be more than twice the depth flow and thus run over the sidewalls. This is important for the design of chute walls in chute spillways with control gates. In this study, the experimental formation of the shockwaves and their behavior along the chute and their reduction measures are presented. Experiments were conducted on a scaled physical model (1/50) of Kheirabad Dam, Water Research Institute, Iran. It was realized that apart from the geometry of piers and chute spillway, Froude number of flow and gate opening are the main effective parameters on the hydraulic performance of shockwaves' formation and their development on gated spillways.

1. Introduction

Spillways are one of the most significant structures of high or small dams that are responsible for discharging the excessive flood flow of the reservoir. Their flow hydraulic characteristics have drawn the attention of many researchers. These characteristics are high velocity, pressure loss, cavitation probability, and aeration. In this regard, several studies have investigated the above-mentioned issues [1–5]. In the spillways, gates are mounted on the crest of a free spillway that controls the head, discharge, reservoir volume and, reservoir level increase. The addition of these gates adds some new complex issues to the hydraulic subjects [6, 7]. Al-Mansori et al. [8] found that, with increasing hydraulic head, up to seven times that of the design head, the flow separation zone grows linearly. Discharge coefficients are studied for a wide range of head ratios. It is concluded that increasing head ratio up to five leads to an increase in the discharge coefficient due to decreasing pressure on the ogee crest. Yang et al. [9] focused on the underlying influence of the air-water momentum exchange in the two-phase Two-Fluid Model. It is modified to better represent the drag force acting on a group of air bubbles and the wall lubrication force accounting for near-wall phase interactions. Samadi et al. [10] and Sylvain and Claire-Eleuthèriane [11] studied the multivariate adaptive regression splines (MARS) approach that has been adopted as a new soft computing tool for estimating the equilibrium scour depth below free overfall spillways. Khalifehei et al. [12, 13] studies investigated the stability of sediment particles using A-Jack concrete block armors. In this regard, the general forms of the incipient motion and incipient failure of A-Jack armor were extracted based on dimensional analysis and particle stability analysis. Karalar and Cavusli [14] studies aimed to examine the nonlinear

seismic behaviors of concrete gravity (CG) dams considering various epicenter distances. For this purpose, Boyabat CG dam that is one of the biggest concrete gravity dams in Turkey is selected as a numerical application. Karalar and Çavuşli [15] studies observed how the time-dependent displacement and stress behavior of a concrete-faced rockfill (CFR) dam change by the effect of the normal and shear interaction spring stiffness parameters. Ilısu Dam that is the longest concrete-faced rockfill dam in the world now and has been completed in the year 2017 is selected for the three-dimensional (3D) creep analyses.

Among gate discharge coefficient, gates location above the spillways, and separation of flow profile, the spillway transverse flows and waves are less known issues. These waves are called by different names such as shockwaves, lateral shockwaves, and rooster tail waves [16–18]. Their height is greater than the average. Additionally, they have a transverse velocity component. Thereupon, the shockwaves' flow moves from one side to the other, imposing a new hydraulic condition to which less attention is being given.

Despite many studies on the hydraulic characteristics of flow in chute spillway, there is insufficient knowledge of the formation of shockwaves. Investigations on the formation of the shockwaves flow in a horizontal rectangular channel by Reinaur and Hager [19] showed that, for the state of constant flow depth h0 and constant pier width bp, the height of waves 1 and 2 and their width increase with increasing of the Froude number. They also showed that wave 1 height was only a function of the ratio of the flow depth to the pier width H_o/b_p. The wave 1 height and wavelength increase by the Froude number increment. In 1997, Reinaur and Hager continued their previous studies on a chute spillway. They observed that if the depth measurements were taken perpendicularly to the chute spillway, the results would be consistent with the studies performed in the horizontal channel [20–22]. In 1998, they also investigated the effects of chute lateral wall convergence and chute floor slope on the rooster tail waves. They suggested a method for reducing transverse waves and designing lateral walls of a chute [23, 24]. In another study, investigations on this type of flow were presented as the standing wave analysis in a chute spillway [25, 26]. Further studies on the shockwaves flow in an aeration chute spillway have shown that the deployment of the aeration intensifies the shockwaves. The waves become larger with the increase of the Froude number [27, 28]. Wu et al. [29] conducted experiments to study shockwaves characteristics. The results revealed that the ratio of the lateral cavity length to the bottom cavity length had a dominant bearing on the intensities of the rooster tail. For the third type of shockwaves, Duan [30] developed a submerged sloping-tail pier for the deep hole gate of the chute of a hydroelectric project to eliminate the shockwaves. The principle and construction of a pier for eliminating the shockwaves were discussed. Reinauer and Hager [19, 22] found that shockwaves characteristics only depended on the ratio of approach flow depth to pier width in a series of experiments conducted in a horizontal channel and sloping chutes. Wu and Yan [31] and Smajdorová and Noskievičová [32] investigated the hydraulic characteristics of the shockwaves induced by the pier of the discharge tunnel of the Sanbanxi hydropower station. It was observed that the primary reason for the shockwaves inception was the concavity of the water surface. Based on that, a new type of pier with a bottom underlay to control the shockwaves for the discharge tunnel was designed [31, 33].

The shockwaves are a parabolic roller flow that occurs in hydraulic structures under various conditions. The shockwaves flow occurs at the downstream piers of the chute gate, downstream arches of the tunnel spillways, the entrance of the bottom outlet tunnel, and the wall of the converging chute [34, 35]. The use of piers is inevitable due to the gates and bridges passage located on the crest of spillways. After passing the dam crest and piers, the supercritical flow of two sides of the pier collides and creates the standing wave at the downstream. These waves, known as pier waves, are referred to as wave 1 in this research. The wave in the form of the shockwaves of type 1 is formed based on the number of intermediate piers located on the spillways. Due to the interaction of these waves, they form regular geometric shapes of rhombic or other types over the spillway water surface (Figure 1). It should be noted that dotted lines are the place where shockwaves form.

Figure 1 shows the plan and schematic longitudinal cross section of the shockwaves flow at the downstream of the symmetric piers. The flow geometry and 3 waves formed on the spillways are shown while all the gates are open. Sections 1, 2, and 3 are the peak of the first, second, and third waves, respectively. In the middle of the spillway, the interference of wave 1 generated a larger one. In this study, this new wave is called wave 2 (Figure 1, section 2). Wave 2 also moves in the direction of the spillway width. In the following, the wave 2 impact on the wall of the chutes produced a new wave which is called wave 3 in this study (Figure 1, section 3). The chutes design and structures exposed to these flows should include the quantitative and qualitative identification of the above-mentioned waves and their detrimental effects on the performance of the spillway structure and in particular its walls [36]. Therefore, identifying their formation location, the characteristics of these waves, evaluating their pressure field and its variations, were considered as significant design hydraulic parameters. This information will considerably assist the designers of these structures.

Studying the shockwaves at the control point $x = 0$ (Figure 1), H_0, v_0, and $Fr = v_o/\sqrt{gH_o}$ are called flow depth, velocity depth, and the Froude number, respectively. The flow geometric parameters are the following: maximum flow depth H_m, flow width at the maximum flow depth location B_m, angle of pier waves formation α, pier width b_p, axial distance of piers b_a and the wave location relative to the control point x. A cavity is created behind the pier from section $X = 0$ to the initial point of wave 1 $X = X_{1i}$. Depending on the flow velocity, the cavity may be submerged or dry (Figure 2). At a distance of $X = 0$ to $X = X_{1i}$, the flow passing through the two sides of the pier collides like two jets and generates the first type of pier waves. This wave is a roller that reaches the maximum wave height (H_{1m}) at X_{1m} by excluding some of the water jets from the main core flow. At the endpoint of type 1 wave (X_{1e}), the core isolated from the

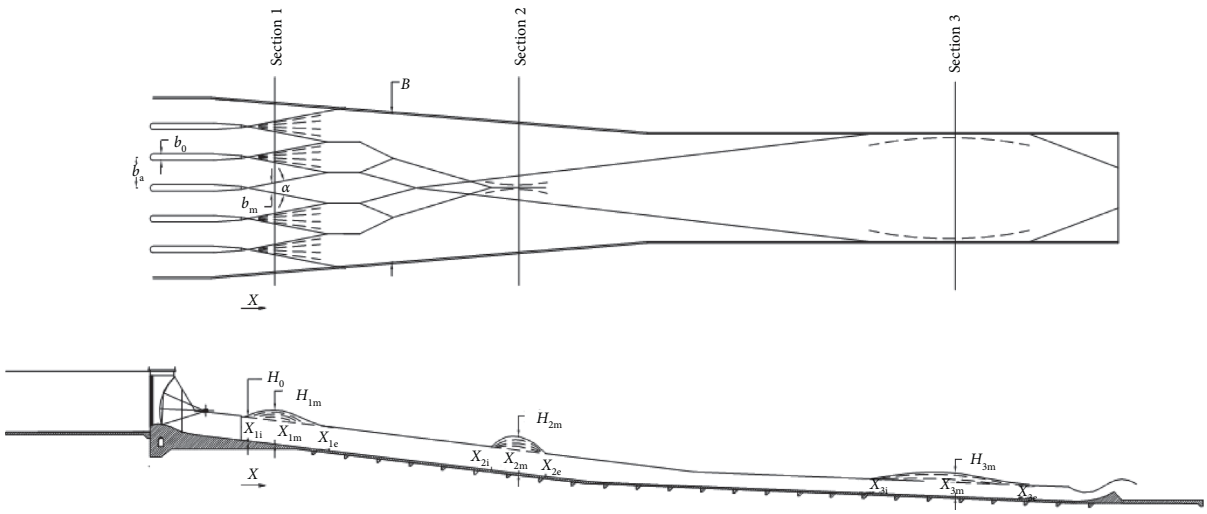

Figure 1: Waves at the downstream of pier chutes: (a) plan and (b) flow longitudinal section (the Kheirabad Dam is located in Khuzestan Province, Iran).

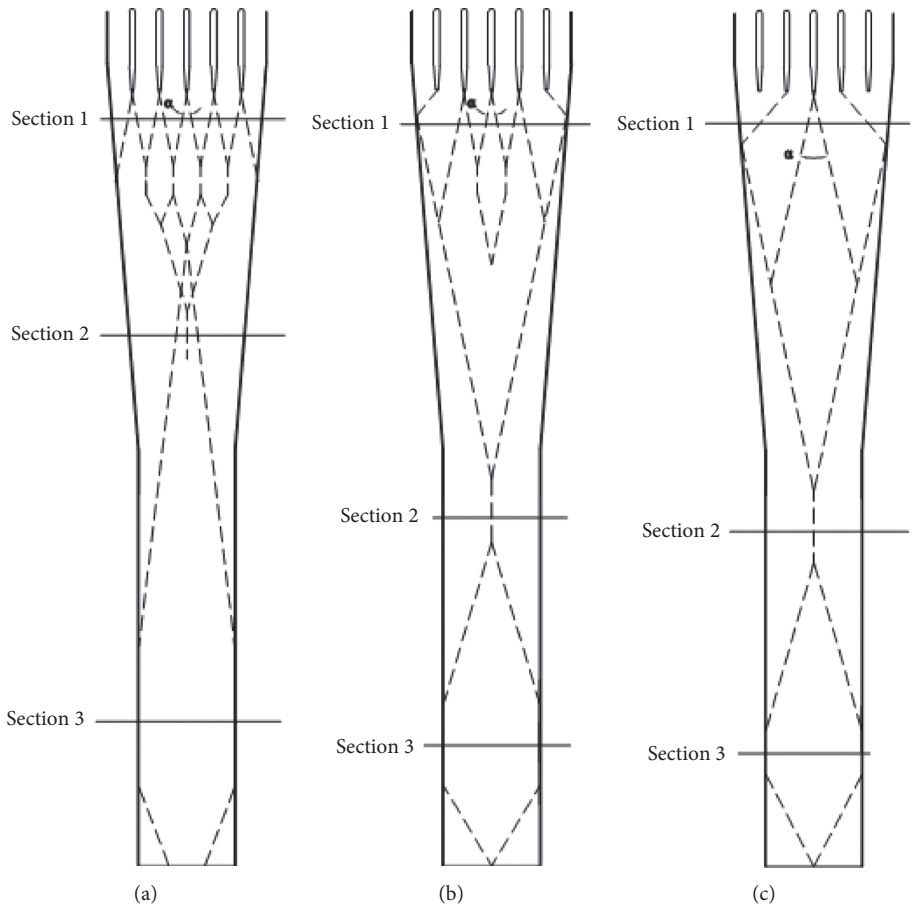

Figure 2: Flow geometric plan under the gates performances. (1) Six gates; (2) four middle gates; (3) two middle gates.

water jets falls to the side of the water padding. Because of wave collision and also due to the convergence of the lateral walls of the spillway, type 1 waves form a wave flow with regular shapes above the spillway. At the end of these shapes (location x_{2i}), wave type 2 is formed. This wave is observed at a maximum height of H_{2m}. Because of the interference of the waves over the spillway as well as the transverse movement of wave 2 at the farther downstream, a wave on the wall or a third wave also forms on the lateral wall of the spillway. Type 3 wave starts from the location $X = X_{3i}$ on the wall and

reaches the maximum height H_{3m} at $X = X_{3m}$ and then disappears into the mainstream at $X = X_{3e}$.

Investigations on hydraulic models of chute spillway at the Iranian Water Research Institute similarly confirm these issues [37]. Based on the observations, by crossing through each aeration, the waves intensify and their height increases. Therefore, these waves' intensity at the chute downstream with some surface aeration is significant. They require being accurately evaluated and mitigated if necessary. Kavianpour et al. [38] mentioned these results investigating the longitudinal and transverse profiles of shockwaves. They suggested a method to reduce these waves. They also showed that the shockwaves flow field over the spillway is a function of the Froude number, gate opening, head values over the spillway, spillway convergence, and pier geometry. Each of these factors can influence the flow field and cause adverse hydraulic conditions on the spillway. Figure 3 shows the flow geometry because of the 2, 4, and 6 middle gates opening. As can be seen, the flow geometry becomes more complex as the number of gate's performance increases. In this study, the shockwaves flow geometry over the spillway, the longitudinal and transverse profiles of the triple waves, and the static pressure of the shockwaves flow field are investigated. It should be noted that dotted lines are the place where shockwaves form.

In practical dam construction projects, ogee spillways with spindle-shaped, ellipse-shaped, or rectangle-shaped piers are most commonly used. Nevertheless, as mentioned before, there is a lack of knowledge on the shockwave for spillways, and most previous studies were conducted for specific dam construction projects, which limit their general applicability. It is, therefore, necessary to investigate the formation and characteristics of the shockwave. This article studies shockwaves formation in an ogee spillway along with a chute channel by physical experiments (scale 1 : 50). A formula for shockwaves height in a slope chute spillway with spindle-shaped or ellipse-shaped piers is also promoted. The causes of the shockwaves behind the pier of the chute spillway were analyzed at the same time. In addition, the conditions for the formation of shockwaves on the spillways have been analyzed at different gate openings.

2. Model Description and Methodology

The study was performed on the physical model of Kheirabad Dam spillway. The Kheirabad Dam is located in Khuzestan Province, Iran. According to the studies that were performed theoretically on different physical models, it was concluded that the Kheirabad Dam spillway is the best possible option in which the shockwaves flow conditions are clearly formed. The physical model was designed at a scale of 1/50 at the Iranian Water Research Institute. The linear geometric scaling of material, which follows Froude's scaling laws, may lead to very large viscous forces that in turn lead to very small Reynolds (Re) number. Since most flows at prototype are both turbulent and in the hydraulic rough regime, where losses are independent of (R), flows in hydraulic Froude models are often "shifted" to the hydraulic rough regime to better account for losses. When Re in the core is higher than 2000, flow in the structure is turbulent, conforms to the prototype situation, and the viscous scale effects are negligible. In this model, the Reynolds number has been controlled, and Reynolds Number greater than 2000 ($Re > 2000$). The scale effect due to surface tension forces becomes important when water waves are very short or flow depth is less. Surface tension effects must be considered when wave periods are less than 0.35 s and water depth is less than 20 mm [39]. In the present study, it was found that both wave period and flow depth were considerably higher; thus, the scale effects by surface tension forces are negligible.

The experimental model includes ogee and chute spillways with 6 gates and 5 piers. Because of the flow collision to the base, there is a rooster tail or a shockwave flow. The laboratory trial and error obtains the pier section spindle-shaped to reduce the shockwaves' flow height in this section. The pier width is 2.4 cm and reaches 1 cm at the end of the spindle. The spillway pier length is 33.8 cm and the pier distance is 9 cm. The spillway chute consists of two parts, one with a 12% slope and the second with a 4% slope. The spillway width at the 12% slope is 132 cm at the beginning and 80 cm at the end. At the 4% slope, this width is fixed with a value of 80 cm. There is a flip bucket at the end of the chute. Due to the shockwaves flow development, the zigzag and waveforms flows are transversely visible on the flip bucket (see Figure 4).

The study found that the regular geometric wave height on the wall can be up to 2 times the water depth. This condition causes the erosion of the chute sidewalls. Figure 5 shows the spillway and the geometric shapes formed on it. In this spillway, the three maximum waves are significant that can cause hydraulically critical conditions. They can influence the chute wall design. Wave 1 is noticeable at the back of the pier. Wave 2 is prominent in the middle of the overflow length that is a consequence of the impact of the oblique and zigzag flows on the spillway. Wave 3 is noticeable on the chute wall. Figure 5 illustrates the collision of the waves with the pier and the created geometry at the downstream. Figure 6 also shows the 3 created maximum waves, locally.

This paper presents the longitudinal and transverse profile variations of the triple waves for three different discharges and also three different gate openings. In the first case, only the two middle gates are open. In the second condition, the four middle gates are open. Lastly, in the third case, all six gates operate.

In this study, the depth and velocity of the inflow to the spillway are changed by the partial opening of the gates. In this study, the partial opening of the gates changes the depth and velocity of the spillway inflow. This partial opening of the gates allows the ability of increasing the speed, decreasing the depth, and consequently the proper change for the Froude number. Also, the flow field piezometric pressure over the spillway is presented for the two operating modes of 6 and 4 middle gates. They are analyzed for 3 separate openings. A depth gauge measured the wave height and profile. Depth measurement error with the depth gauge is subject to the flow conditions. In the smooth flow without oscillation, the error is ±1 mm. In models of oscillatory flow such as the shockwaves, the error is up to ±5 mm [40, 41].

Figure 3: Interaction effect of jet flow with shockwaves in flip bucket area.

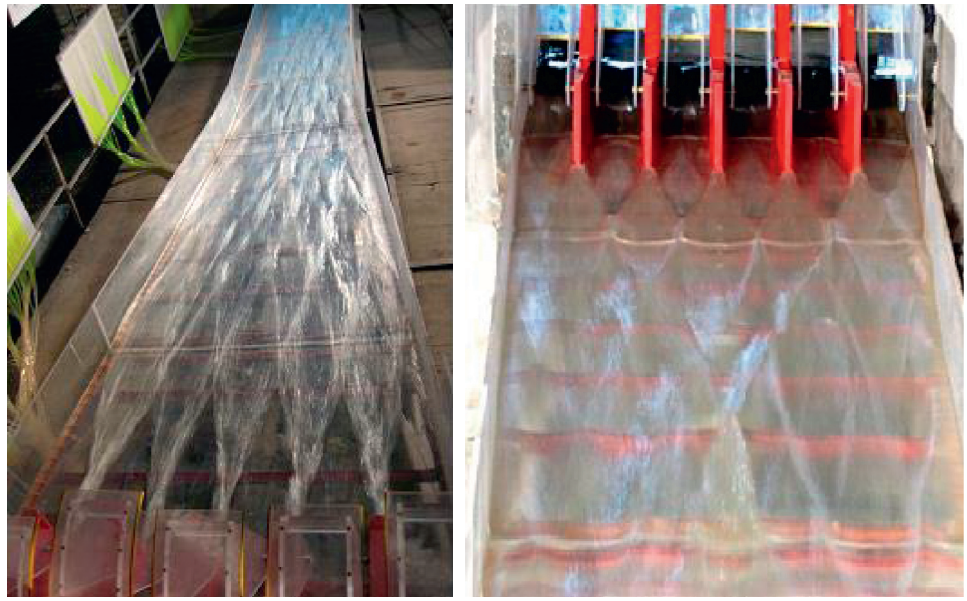

Figure 4: Geometric shapes formed from shockwaves over the chute.

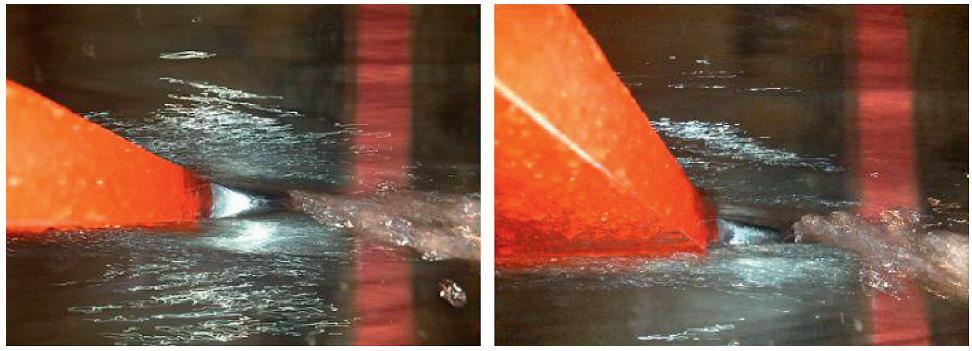

Figure 5: Cavity formation behind the pier.

In the present study, based on the flow conditions and the range of wave height variations, the maximum measurement error is 5%. A piezometer was also used to measure static pressure [42, 43]. The piezometer shows the fluid pressure as the liquid-equivalent height. The control or reference section was two piers between the gates with the "o" index. In this control point, the flow characteristics, the depth H_o, the velocity v_0, and the Froude number (Fr_o) (due to the gate function) were submitted in the table of each experiment. At the control section, the experimental Froude numbers change from 2 to 4. However, the variety of the Froude numbers is much larger at the downstream of the spillway, in the range of 8 to 10.

This research calculates the maximum wave height in terms of efficient parameters on the phenomenon as dimensionless graphs. In the chute spillway, the

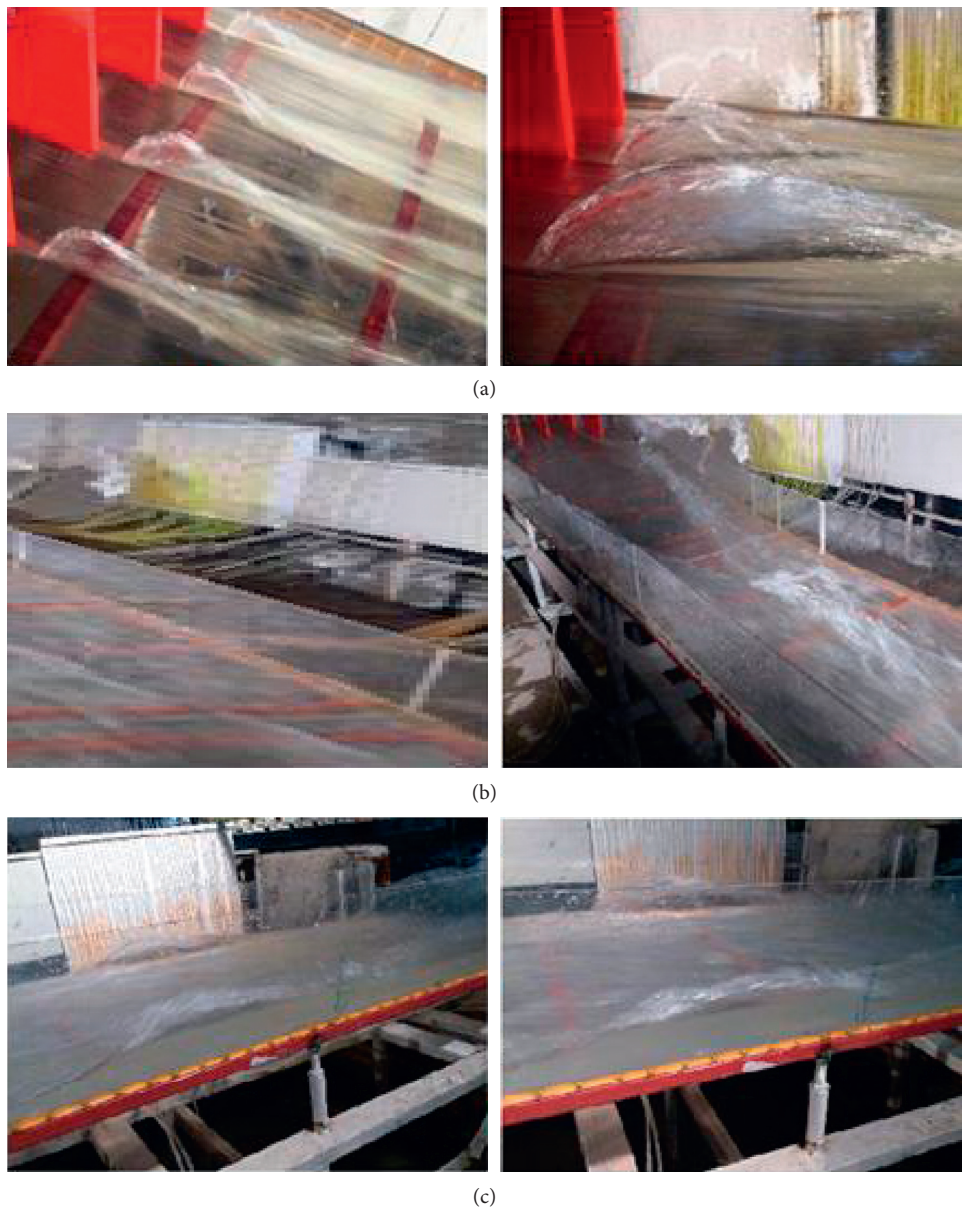

(a)

(b)

(c)

Figure 6: The shockwaves created over the chute. (a) Pier waves or wave 1. (b) Middle wave or wave 2. (c)Wave at the wall or wave 3.

important variables affecting the maximum wave height H_m include the fluid bulk density ρ, the fluid dynamic viscosity μ, the water surface tension coefficient σ, the gravity g, the flow depth at the control section H_o, the flow velocity at the control section v_0, the pier width b_p, the pier axial distance b_a, the spillway sidewall slope θ_w, and the spillway floor slope θ_b. A general function of effective variables on the height of shockwaves can be defined as

$$H_m = f\left(\rho, \mu, \sigma, H_\circ, v_\circ, b_p, b_a, \theta_b, \theta_w, g\right). \quad (1)$$

In the physical model, it was not possible to change the geometrical parameters θ_w, θ_b, b_a, and b_p. As a result, the experiments were performed without any changes in the physical model. Accordingly, these parameters could be extracted from this study's efficient variables. Employing Buckingham's theory, expressing the dimensionless wave maximum height in the form H_m/H_0 and ensuring the flow turbulence during the overflow, the Reynolds number effect is ignored. Additionally, as the water height above the spillway is always greater than 5 mm during the experiment, the Weber number effect is assumed to be negligible. So, H_m/H_0 is calculated as follows [44, 45]:

$$\frac{H_m}{H_\circ} = f\left(Fr_o\right). \quad (2)$$

As can be seen, the dimensionless maximum height is function of the inflow depth H_o and the control section

Froude number Fr_0. In the following, the wave height variations are presented in dimensionless form.

3. Results and Discussion

3.1. Longitudinal and Transverse Wave Profiles. In this section, the longitudinal and transverse profiles of the waves for the operation of two middle gates, 4 mid gates, and 6 gates were investigated. The longitudinal sections are in the direction of the flow. The transverse sections are at the location of the maximum wave height. Figure 7 shows a view of this flow and the triple waves for the opening of the two middle gates. In this case, only one pier causes the formation of shockwaves flow.

Figure 8 illustrates the longitudinal and transverse profiles for the two middle gates' performances. The "a" curves represent 100% gate openings. The "b" curves represent 60% gate openings. The "c" curves represent 30% opening of the gate. It should be noted that all measurements were in the longitudinal direction from the end of the pier. The height of the waves was measured from the spillway floor. Parameter X is coordinated in the spillway direction. Parameter B is the coordinate at the spillway width. According to curve 1 of Figure 8, as the opening increases, the dimensionless height of wave 1 decreases, while its maximum location shifts toward upstream. A comparison of the wave transverse variations is also shown in curve 2 of Figure 8. For wave 2, the same trend is evident in curves of 3 and 4; however, as compared to wave 1, this wave affects only a small portion of the spillway width. Wave 2 dimensionless length increases with the decrease of opening. The trend of decreasing relative height and decreasing the relative distance of the wave peak upstream with the opening is repeated in wave 3 for wave 5. According to Figure 6, these waves only affect the wall region, which is a total of 25% of the spillway width on both sides.

Table 1 presents the flow characteristics for the two gates' operation mode studying waves 1, 2, and 3. According to Table 1, by the gate opening increment, the wave 1 height increases. Besides, its maximum location shifts toward upstream. Wave 2 height reduces by decreasing opening. With the increase in gate opening, the trend of height gain and the upward shift of the wave 3 peak is also noticeable.

Figure 9 shows the longitudinal and transverse profiles when the four middle gates operate. In this figure, the curves d, e, and f illustrate 100%, 60%, and 30% of gates opening, respectively. The flow characteristics of the four intermediate gates and waves 1, 2, and 3 are shown in Table 2.

Except for the number of pier waves, all trends and changes observed in the opening mode of two gates are also valid for the opening of 4 gates. There are three pier waves instead of one pier wave (according to curve 2 of Figure 9). Figure 10 also shows the longitudinal and transverse profiles of the six gates performances. The curves "g", "h," and "i" are 100%, 60%, and 30% openings, respectively. The flow characteristics of the six open gate operating modes and waves 1, 2, and 3 are also presented in Table 3. According to curve 2 of Figure 10, all the trends and differences observed in the two preceding states are also true for the opening of 6 gates, other than the number of the pier waves. Five pier waves have occurred for the opening of 6 gates. However, the height of the pier waves also decreased with the increase of the pier.

As can be seen in Figures 8–10, the Froude number is an important parameter in the shockwaves' wave variation over the spillway. It results from the variation process that, for all three defined waves, the changes are made in the same way by the Froude number. So, the height and location of the wave peak, the end-of-wave cross section, and the pier wave formation angle change with the flow Froude number. As the Froude number increases, the waves get longer and thinner, and the peak and end sections of the wave are shifted toward farther downstream. In general, considering the range of Froude numbers in this study, it is observed that, in the six-gate operation mode, the height of waves 1, 2, and 3 (according to Table 3) is maximum 1.3, 1.5, and 1.3 times the average depth of flow at the same cross section. In the case of the four middle gates operation, these values are 1.4, 1.8, and 1.2, respectively. They are, respectively, 1.5, 2.3, and 2.5 for the two middle gates performance. Moreover, as the Froude number decreases, the wave height increases, the wavelength decreases, and the pier waves formation angle is increased. Separate experiments were performed to illustrate how the pier waves formation angle (α) changes with the Froude number. Figure 11 presents its physical outcomes. Figure 11 shows the results of two Froude numbers $Fr_0 = 2.07$ and 3.1 for a middle pier state. For $Fr_o = 2.07$, the pier wave formation angle (α) is noticeable; pier wave 1 with greater width is created. For $Fr_o = 3.1$, the pier wave formation angle (α) is smaller; the wave is narrower.

For the two increase options and by testing and observing the model flow conditions, to reduce the shape of the shockwaves flow and not affecting the flow behavior during the chute, the best option was selected for the downstream pier shape and stabilized in the model. Figure 12 shows the actual flow conditions for pier end different options at a discharge of 5000 cubic meters per second. By trial and error and observation for several different options, it was observed that, by increasing the pier length and decreasing its end thickness, the formation and skipping of the shockwaves' flow are stabilized in the model. These conditions also depend on structural and executive issues.

Research has recommended the use of pier-mounted blades to reduce the height of the waves so that the point of flow contact moves from the two sides of the pier to the blade tip [19]. This method is not executive and suitable. Changing the pier geometry as recommended in the present article, while applicable, significantly reduces the height of the created shockwaves' flow and decreases the wall wave height by decreasing wave 1 height.

Figure 13 shows the longitudinal sections of the triple waves along the spillway. In all three categories of waves, the process of change is the same in terms of the Froude number. The height of the waves, the location of the wave peak, the cross section of the wave, and the angle of wave

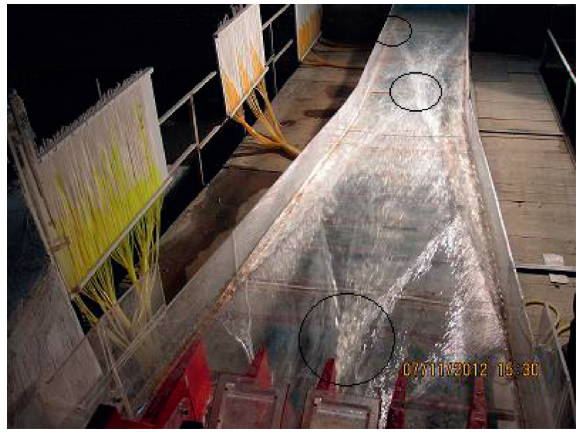

Figure 7: Flow and location of triple waves for two open middle gate modes.

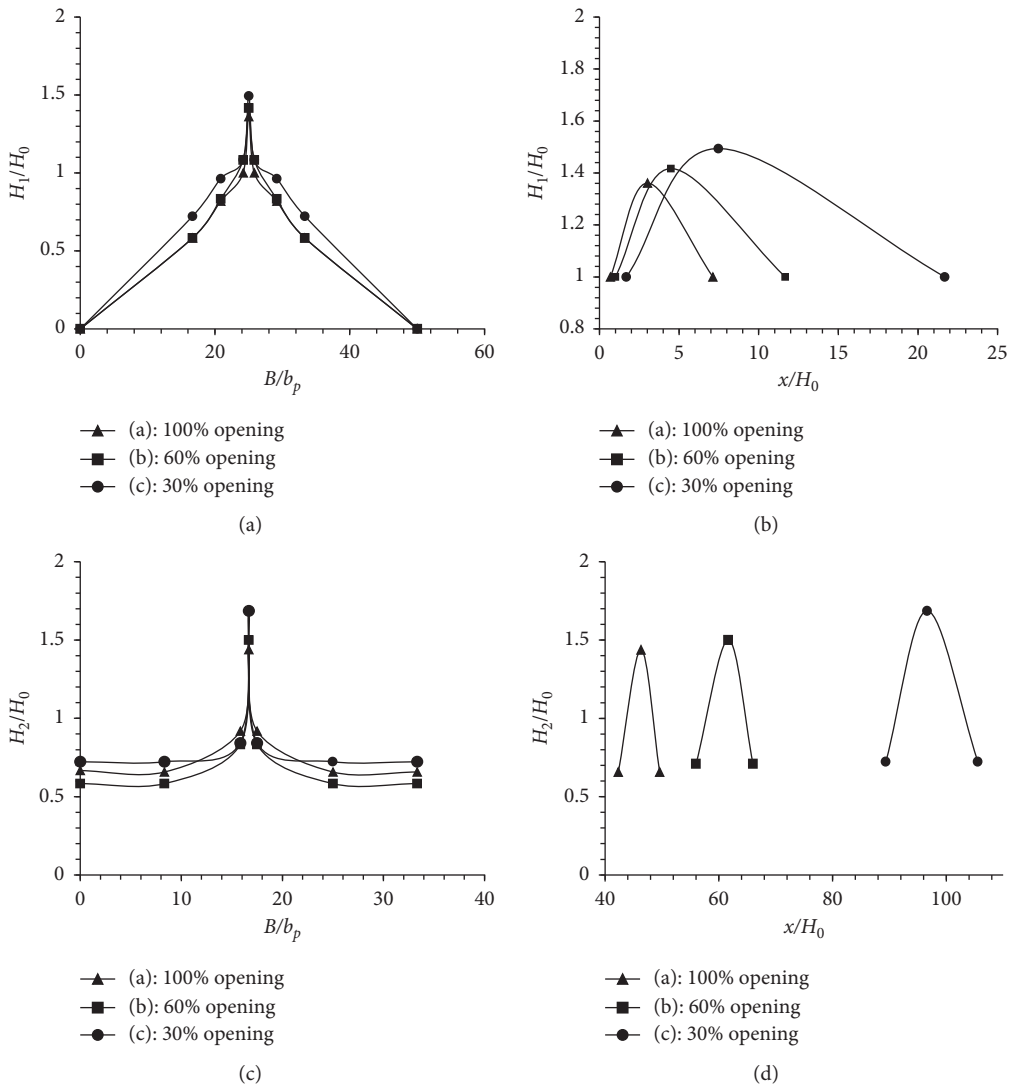

Figure 8: Continued.

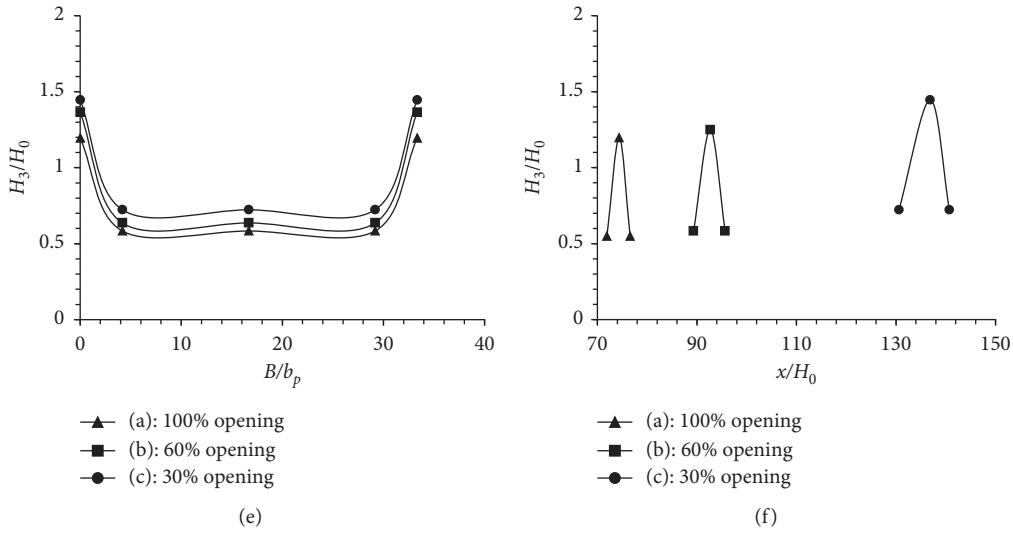

Figure 8: Longitudinal and transverse dimensionless profiles for the two middle gates' performances: (a) wave 1 longitudinal profile, (b) wave 1 transverse profile, (c) wave 2 longitudinal profile, (d) wave 2 transverse profile, (e) wave 3 longitudinal profile, and (f) wave 3 transverse profile.

Table 1: The shockwaves' flow characteristic for two middle gates' operations.

Type	Opening	Wave type	Fr_o	Q (lit/s)	H_m (cm)	X_i (cm)	X_m (cm)	L (cm)	α (degree)	B_m (cm)	
		1			9.6	5	22	47	32.42	12.5	
a	100%	2	2.05	91.2	10.5	309	338	53	—	—	
		3			8.6	525	543	34	—	—	
		1			8.5	6	27	64	28.37	11.68	
b	60%	2	2.47	60.6	9	336	370	60	—	—	
		3			7.5	536	556	38	—	—	
		1			6	7	31	83	25.61	11.01	
c	30%	2	3.07	44.4		7	370	400	67	—	—
		3				6	542	568	42	—	—

formation vary with the flow Froude number. As can be seen, as the Froude number increases, the length of the wave increases, while its height decreases. Also, the maximum end sections of the wave are moved downstream. The height of the waves depends on the flow depth and their length depends on the flow velocity. As a result, as the depth of flow increases; the height of the wave increases. Moreover, as the velocity of flow increases, the length of the waves increases. Also, with increasing the gates opening, the flow depth increases while the Froude number decreases. Consequently, the wave height increases while the wavelength decreases. The maximum end sections also move upstream. Also, by investigating the transverse sections of the waves, increasing the Froude number makes the waves narrower while the waves become wider by decreasing the Froude number. As can be seen in Figure 13, wave 2 (the spillways' middle wave) is much higher than the other two waves. Then, wave 3 and wave 1 are next in terms of height.

Figure 14 shows the location of the triple wave formation over the spillway plan. Wave 2 is formed over a broader range of spillway. The range of wave 3 formation is very critical because the wall wave is a shockwave that exerts considerable dynamic pressure on the sidewall of the chute. On the contrary, the height of these waves can be larger than the height of the chute wall. Subsequently, wave 3 (wall wave) is essential from a design viewpoint.

Figure 15 shows the dimensionless curves of the maximum height of waves 1, 2, and 3 and their location of formation in terms of the Froude number for two, four, and six gate operations. For different operations of the gates, the height of all the waves and their longitudinal coordinates have a clear and relatively linear trend in terms of the Froude numbers. Figure 16 also shows the dimensionless curve of the wave 1 formation angle in terms of the Froude number. As the Froude number increases, the angle α decreases linearly, making the waves sharper and thinner.

3.2. Piezometric Pressure. The piezometric pressure distributions of the spillway floor were measured and given beneath the height maximum location and landing point of waves 1 and 2 as well as the place of wave 3 peaks on the walls. Considering two modes of six gates and four middle gates operating, Figures 17 and 18 show the piezometric pressure coefficient distribution of triple waves for the three

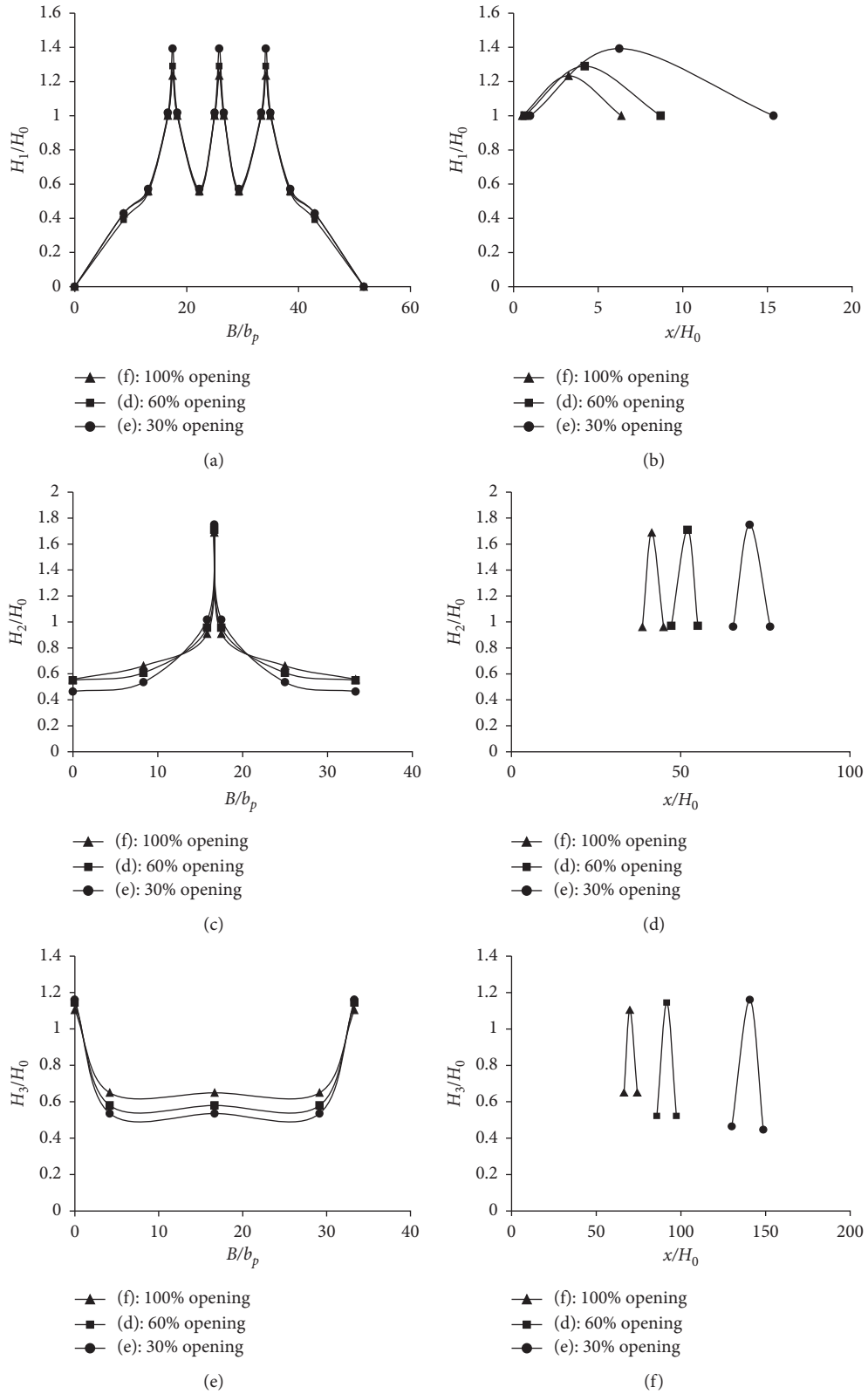

Figure 9: Longitudinal and transverse dimensionless profiles of waves for the four gates' performances.

openings 100%, 60%, and 30% with corresponding input Froude numbers. The vertical axis represents the pressure coefficient. In the control section, the pressure coefficient is dimensionless relative to the velocity head in the form of $c_p = (p/(V^2/2g))$. The horizontal axis also indicates the longitudinal distance of the points from the pier beginning.

Table 2: The shockwaves' flow characteristic for four middle gates' operations.

Type	Opening	Wave type	Fr_o	Q (lit/s)	H_m (cm)	X_i (cm)	X_m (cm)	L (cm)	α (degree)	B_m (cm)
		1			9.3	4	25	45	22.62	9.8
d	100%	2	2.1	126	14.1	298	349	48	—	—
		3			8.9	485	510	57	—	—
		1			8.5	4.5	29	55.5	19.87	8.22
e	60%	2	2.75	90.6	11.5	326	359	54	—	—
		3			7.7	515	550	69	—	—
		1			7.5	5.5	25	80.5	17.65	6.06
f	30%	2	3.9	62.4	8	367	394	61	—	—
		3			5.5	540	584	77	—	—

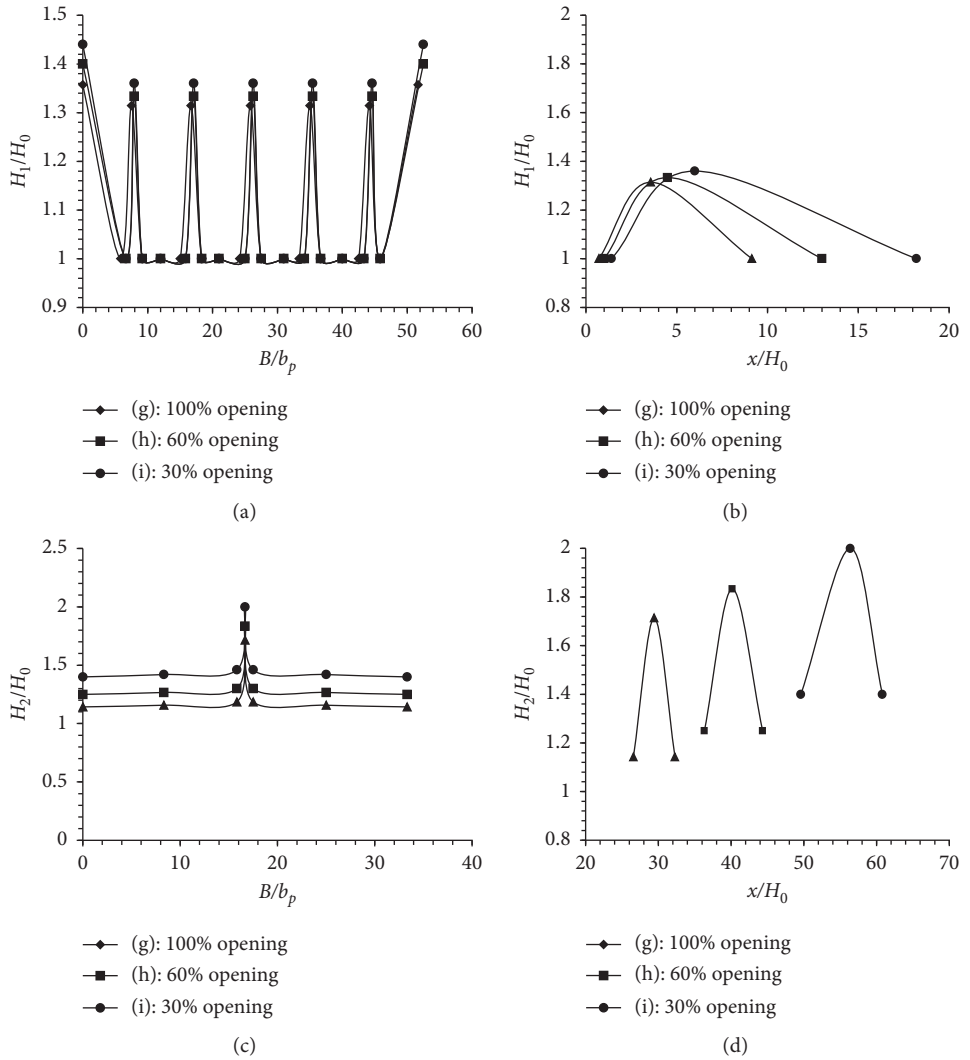

Figure 10: Continued.

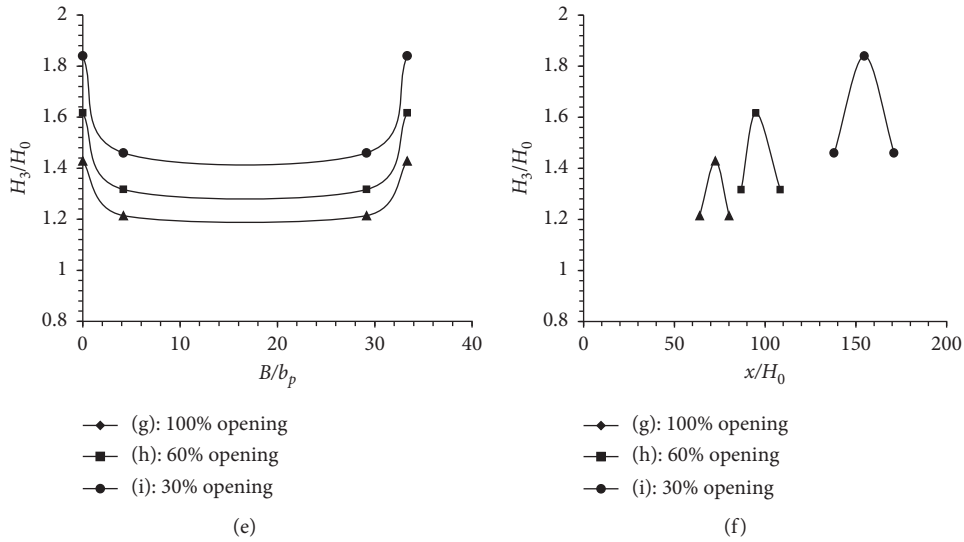

Figure 10: Longitudinal and transverse dimensionless profiles of waves for the six gates' performances; 1: longitudinal profile of wave 1.

Table 3: The shockwaves' flow characteristic for six middle gates' operations.

Type	Opening	Wave type	Fr_o	Q (lit/s)	H_m (cm)	X_i (cm)	X_m (cm)	L (cm)	α (degree)	B_m (cm)
g	100%	1	2.18	209.6	9.2	5	25	59	22.17	7.73
		2			12	186	206	40	—	—
		3			10	467	530	118	—	—
h	60%	1	3.1	125.8	8	6	27	72	16	5.88
		2			11	218	241	48	—	—
		3			9.7	521	570	99	—	—
i	30%	1	3.7	83.8	6.8	7	30	84	12.1	3.64
		2			10	248	282	56	—	—
		3			9.2	573	608	77	—	—

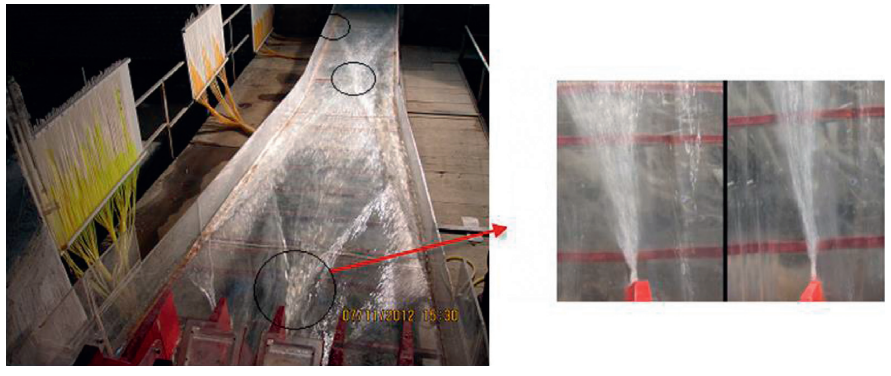

(a) (b)

Figure 11: Wave 1 plan view: (a) $Fr_o = 3.1$ and (b) $Fr_o = 2.07$.

In these curves, the points from the left are, respectively, the location of the peak height and the landing point of wave 1 and 2 and the location of the peak wave 3 height formation on the spillway wall.

As shown, the piezometric pressure decreased as the water height decreased at the landing point of wave 1 relative to its maximum height point. In the following, as wave 2 height is higher than wave 1, the piezometric pressure increases. According to Figure 19, wave 2 is separated from the core of water over the spillway at the peak point. Likewise, as the water level rises at the landing point, the piezometric pressure is increased. The flow also hits the spillway sidewall

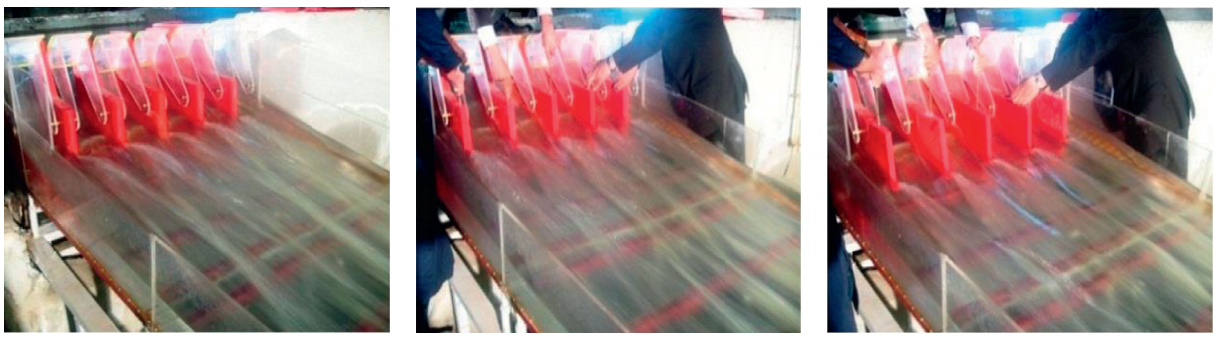

(a) (b) (c)

Figure 12: The shockwaves jump for different options at 5000 cubic meters per second: (a) initial plan, (b) first option, and (c) third option-final one.

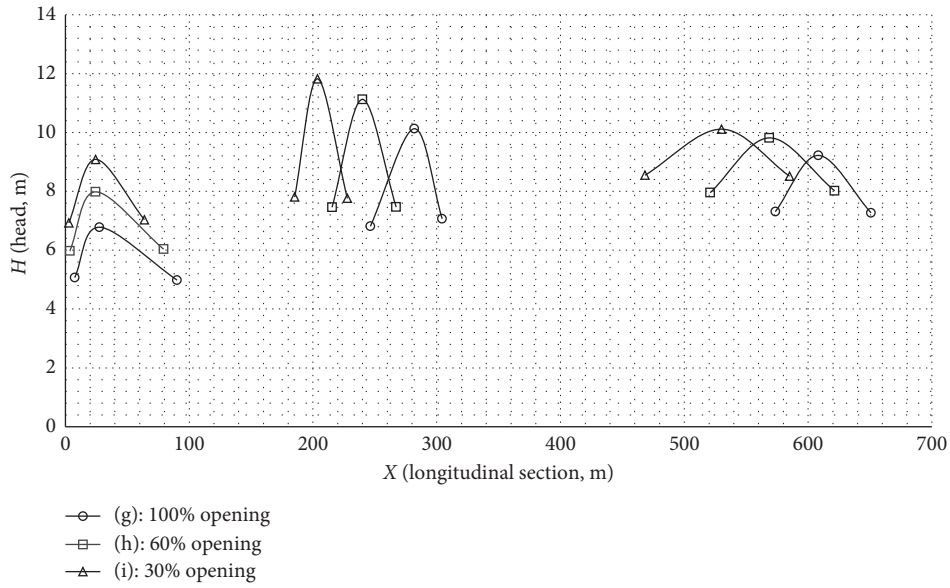

Figure 13: Waves 1, 2, and 3 variation along the spillway in terms of different openings and Froude number.

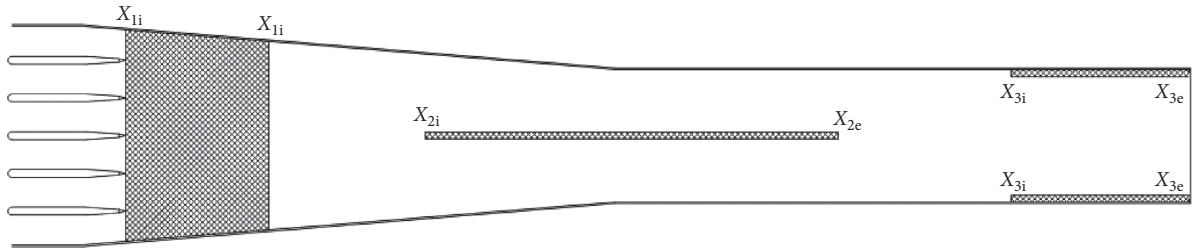

Figure 14: Location of the triple wave formation.

strongly at the location of wave 3 peak height; the piezometric pressure reaches its maximum value. As mentioned, by increasing the number of the Froude number and decreasing the percentage of gate openings, the height of the waves decreases while the waves become longer. Therefore, according to Figures 17 and 18, the piezometric pressure decreases with increasing input Froude number. Also, at the fixed opening for all gate performance modes, the pressure at the location of maximum wave 1 height is higher than that of wave landing, which is the opposite of wave 2. For wave 2, the pressure at the landing point is greater than its maximum height location.

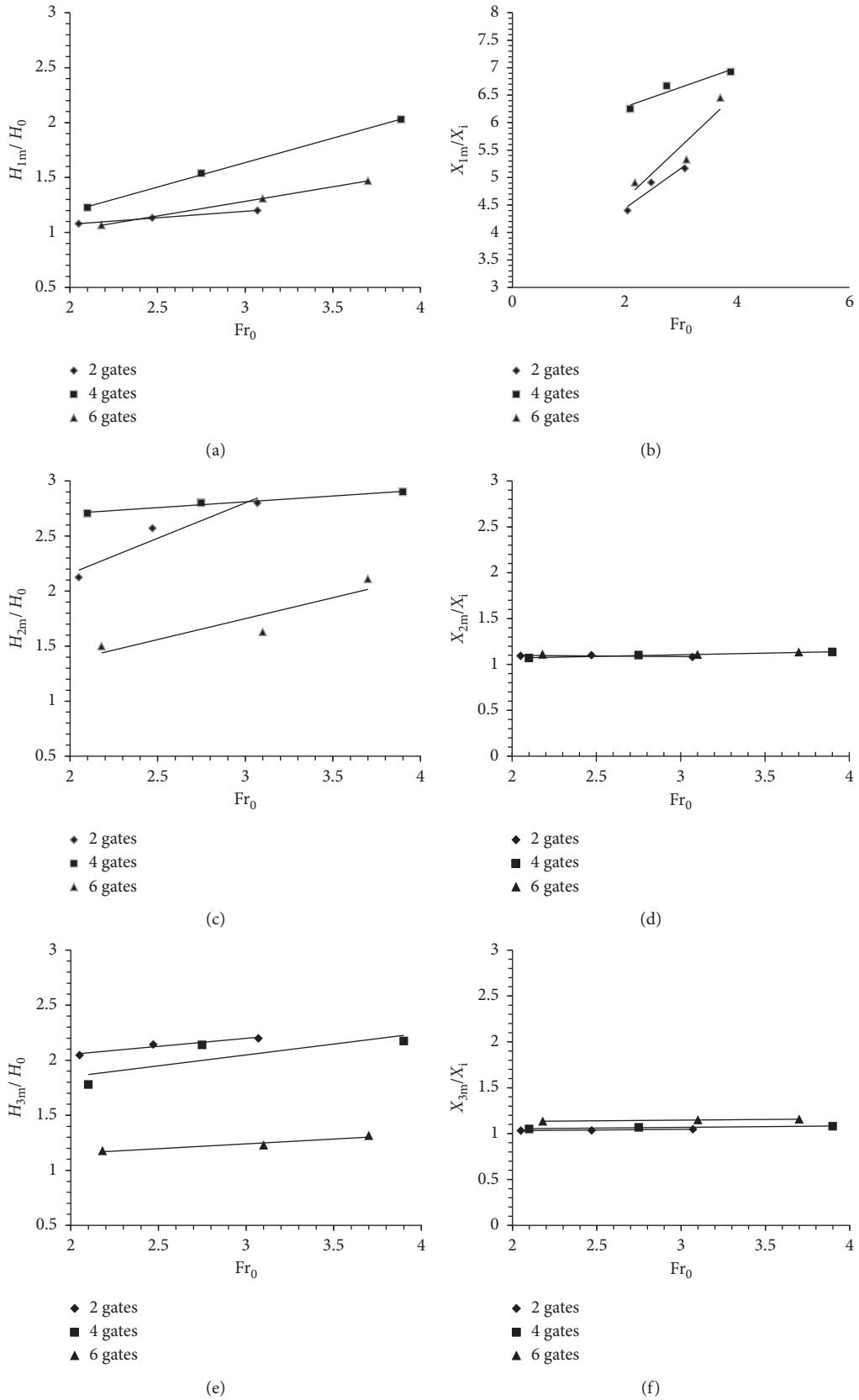

Figure 15: Dimensionless curves of maximum height variation and their formation location in terms of the Froude number for different gate performances.

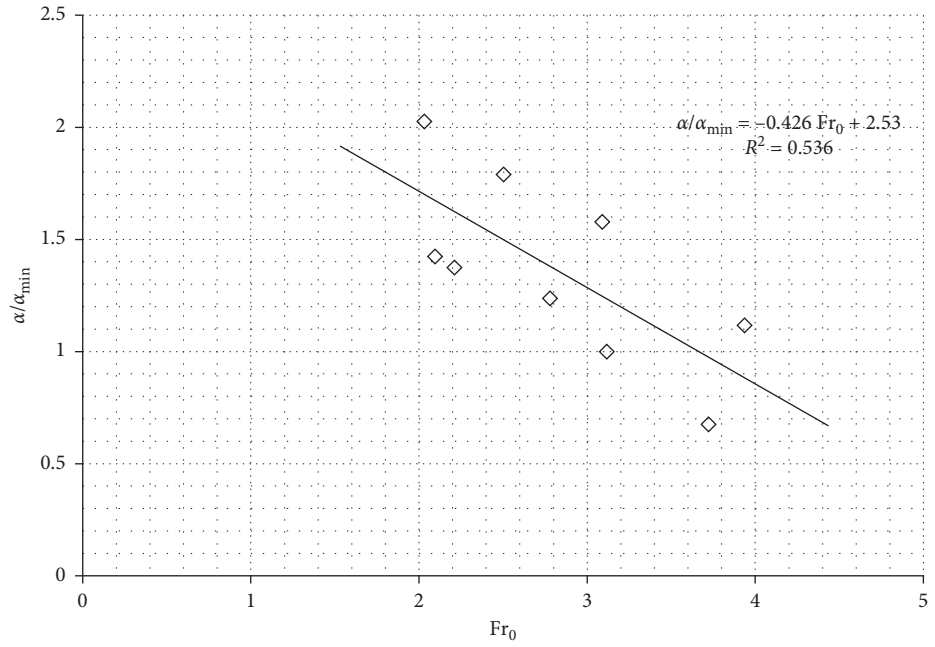

Figure 16: Dimensionless curves of the wave formation angle variation in terms of the Froude number.

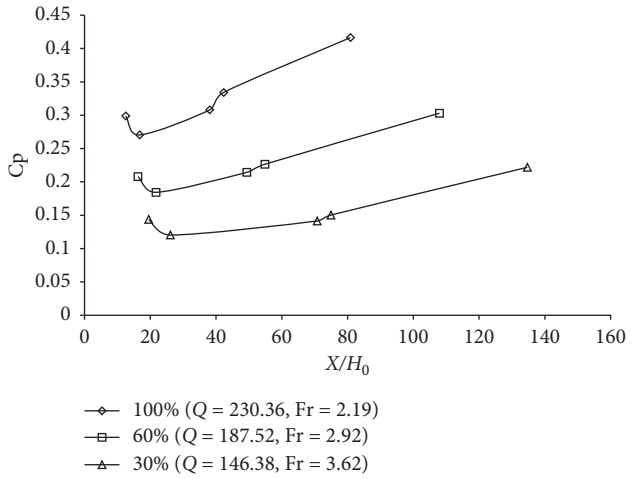

Figure 17: Piezometric pressure head distribution of triple waves for the performance of six middle gates' operation.

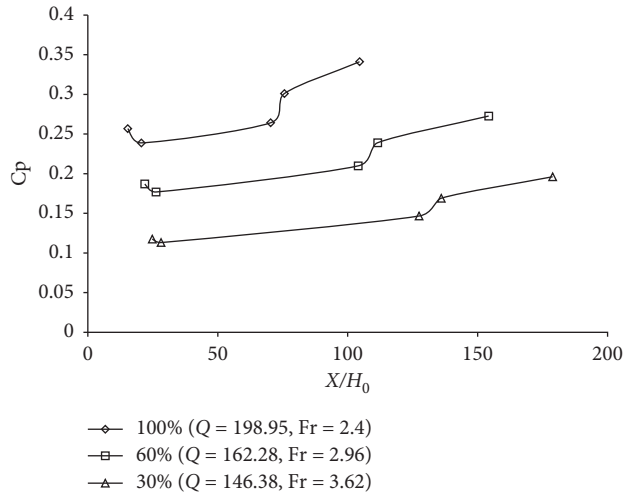

Figure 18: Piezometric pressure head distribution of triple waves for the performance of four middle gates' operation.

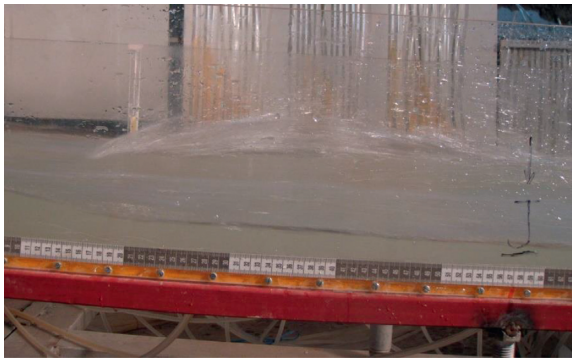

Figure 19: Separation of wave 2 from the main core of water flow.

4. Conclusion

At the downstream of the gates or bridge over the chute spillway, the supercritical flow generates standing waves, named shockwaves or rooster tail waves. The shockwaves' flow influences the flow field and hydraulic condition over the spillway as well as damages the walls of the spillway. Hydraulic flow conditions include the transverse and longitudinal distribution of velocity, pressure, and momentum, which can affect the hydraulic performance of the spillway structure, its structural design, and its dimensions and size. They were studied in three categories of waves 1, 2, and 3. Wave formation on the chute wall is also noteworthy because of its effect on the design process.

As the Froude number increases, the length of waves at the walls becomes longer, the wave height becomes shorter, and the waves are thinner. The maximum end sections of the wave are transmitted downstream. As the Froude number increases, the waves 1 and 2 become thinner while the waves get broader as the Froude number decreases. Wave 2 or spillway middle flow is higher than the other two waves. Next, wave 3 is higher than wave 1. Wave 2 is created over a broader range of the spillway. The wave at the spillway wall is a shockwave that exerts noticeable dynamic pressure on the chute sidewall. In this regard, the wave height can be bigger than the chute wall height. The height of all waves and their longitudinal coordinates represent a linear trend in terms of Froude numbers. Wave 1 has the highest while wave 2 has the least variation relative to the Froude number. By reducing the opening of the gates and consequently increasing the Froude number, the piezometric pressure decreases. At a fixed opening for each of the gate performance modes, the piezometric pressure of wave 3 is higher than the rest. The piezometric pressure of wave 2 is similarly higher than wave 1.

Data Availability

All the data used to support the findings of this study are included within the article.

Conflicts of Interest

The authors declare that they have no conflicts of interest.

References

[1] J. Lucas, W. H. Hager, and R. M. Boes, "Deflector effect on chute flow," *Journal of Hydraulic Engineering*, vol. 139, no. 4, pp. 444–449, 2013.

[2] K. W. Frizell, F. M. RennSa, and J. Matos, "Cavitation potential of flow on stepped spillways," *Journal of Hydraulic Engineering*, vol. 139, no. 6, pp. 630–636, 2013.

[3] M. Pfister, J. Lucas, and W. H. Hager, "Chute aerators: preaerated approach flow," *Journal of Hydraulic Engineering*, vol. 137, no. 11, pp. 1452–1461, 2011.

[4] P. Novak, A. I. B. Moffat, C. Nalluri, and R. Narayanan, *Hydraulic Structures*, Springer, Berlin, Germany, 4th edition, 2007.

[5] P. F. Borowski, "New technologies and innovative solutions in the development strategies of energy enterprises," *HighTech and Innovation Journal*, vol. 1, no. 2, pp. 39–58, 2020.

[6] K.-H. Lee, "Simulation of dam-breach outflow hydrographs using water level variations," *Water Resources Management*, vol. 33, no. 11, pp. 3781–3797, 2019.

[7] E. Eghlidi, G. A. Barani, and K. Qaderi, "Laboratory investigation of stilling basin slope effect on bed scour at downstream of stepped spillway: physical modeling of javeh RCC dam," *Water Resources Management*, vol. 34, pp. 1–14, 2019.

[8] N. J. H. Al-Mansori, N. J. Hussien, T. J. Mizhir Alfatlawi, T. J. M. Alfatlawi, and K. S. Hashim, "effects of different shaped baffle blocks on the energy dissipation," *Civil Engineering Journal*, vol. 6, no. 5, pp. 961–973, 2020.

[9] J. Al-Zubaidi, P. Teng, and H. Zhang, "Experiments and CFD modeling of high-velocity two-phase flows in a large chute aerator facility," *Engineering Applications of Computational Fluid Mechanics*, vol. 13, no. 1, pp. 48–66, 2019.

[10] M. Samadi, E. Jabbari, H. M. Azamathulla, and M. Mojallal, "Estimation of scour depth below free overfall spillways using multivariate adaptive regression splines and artificial neural networks," *Engineering Applications of Computational Fluid Mechanics*, vol. 9, no. 1, pp. 291–300, 2015.

[11] G. Sylvain and G. Claire-Eleuthèriane, "Overcoming the obstacle of time-dependent model output for statistical analysis by nonlinear methods," *HighTech and Innovation Journal*, vol. 2, no. 1, pp. 1–8, 2020.

[12] K. Khalifehei, G. Azizyan, M. Shafai-Bajestan, and K. W. Chau, "Experimental modeling and evaluation sediment scouring in riverbeds around downstream in flip buckets," *International Journal of Engineering*, vol. 33, no. 10, pp. 1904–1916, 2020.

[13] K. Khalifehei, G. Azizyan, M. Shafai-Bajestan, and K. W. Chau, "Stability of A-Jack concrete block armors protecting the riverbeds," *Ain Shams Engineering Journal*, In Press, 2020.

[14] M. Karalar and M. Cavusli, "Seismic effects of epicenter distance of earthquake on 3D damage performance of CG dams," *Earthquakes and Structures*, vol. 18, no. 2, pp. 201–213, 2020.

[15] M. Karalar and M. Çavuşli, "Effect of normal and shear interaction stiffnesses on three-dimensional viscoplastic creep behaviour of a CFR dam," *Advances in Civil Engineering*, vol. 2018, Article ID 2491652, 17 pages, 2018.

[16] H. Xue, M. Diao, Q. Ma, and H. Sun, "Hydraulic characteristics and reduction measure for rooster tails behind spillway piers," *Arabian Journal for Science and Engineering*, vol. 43, no. 10, pp. 5597–5604, 2018.

[17] V. H. Vayghan, M. Mohammadi, and A. Ranjbar, "Experimental study of the rooster tail jump and end sill in horseshoe

spillways," *Civil Engineering Journal*, vol. 5, no. 4, pp. 871–880, 2019.

[18] S. Jung, S. Peetz, and M. Koch, "Poeam - a method for the Part Orientation evaluation for additive manufacturing," *HighTech and Innovation Journal*, vol. 1, no. 1, pp. 21–27, 2020.

[19] R. Reinauer and W. H. Hager, "Supercritical flow behind chute piers," *Journal of Hydraulic Engineering*, vol. 120, no. 11, pp. 1292–1308, 1994.

[20] F. B. Becerro, "Phraseological variations in medical-pharmaceutical terminology and its applications for English and German into Spanish translations," *SciMedicine Journal*, vol. 2, no. 1, pp. 22–29, 2020.

[21] M. G. Mooselu, M. R. Nikoo, N. B. Rayani, and A. Izady, "Fuzzy multi-objective simulation-optimization of stepped spillways considering flood uncertainty," *Water Resources Management*, vol. 33, no. 7, pp. 2261–2275, 2019.

[22] R. Reinauer and W. H. Hager, "Pier waves in sloping chutes," *International Journal on Hydropower & Dams*, vol. 4, no. 3, pp. 100–103, 1997.

[23] R. Reinauer and W. H. Hager, "Supercritical flow in chute contraction," *Journal of Hydraulic Engineering*, vol. 124, no. 1, pp. 55–64, 1998.

[24] B. A. Parate, "Propellant actuated device for parachute deployment during seat ejection for an aircraft application," *HighTech and Innovation Journal*, vol. 1, no. 3, pp. 112–120, 2020.

[25] W. H. Hager and A. J. Schleiss, *Constructions Hydrauliques*, Presses Polytechniques Et Universitaires Romandes (PPUR), Lausanne, Switzerland, 2009.

[26] O. A. Yamini, M. R. Kavianpour, and A. Movahedi, "Pressure distribution on the bed of the compound flip buckets," *The Journal of Computational Multiphase Flows*, vol. 7, no. 3, pp. 181–194, 2015.

[27] S. Pagliara, S. M. Kurdistani, and T. Roshni, "Rooster tail wave hydraulics of chutes," *Journal of Hydraulic Engineering*, vol. 137, no. 9, pp. 1085–1088, 2011.

[28] K. Ha, "Innovative blade trailing edge flap design concept using flexible torsion bar and worm drive," *HighTech and Innovation Journal*, vol. 1, no. 3, pp. 101–106, 2020.

[29] J.-H. Wu, D. Li, F. Ma, and S.-T. Qian, "Fin characteristics of aerator devices with lateral deflectors," *Journal of Hydrodynamics*, vol. 25, no. 2, pp. 258–263, 2013.

[30] W. J. Duan, "The submerged sloping-tail pier—an effective measure to eliminate the crown of jumping flow," *Journal of Sichuan University: Engineering Science Edition's*, vol. 1, pp. 63–67, 1982, in Chinese.

[31] J.-H. Wu and Z.-M. Yan, "Hydraulic characteristics of bottom underlay-type pier for water-wing control," *Journal of Hydrodynamics*, vol. 20, no. 6, pp. 735–740, 2008.

[32] T. Smajdorová and D. Noskievičová, "Methodology for the application of nonparametric control charts into practice," *Emerging Science Journal*, vol. 4, no. 4, pp. 272–282, 2020.

[33] G. Mihajlović and M. Živković, "Sieving extremely wet earth mass by means of oscillatory transporting platform," *Emerging Science Journal*, vol. 4, no. 3, 2020.

[34] A. R. Sengupta, R. Gupta, and A. Biswas, "Computational fluid dynamics analysis of stove systems for cooking and drying of muga silk," *Emerging Science Journal*, vol. 3, no. 5, pp. 285–292, 2019.

[35] S. R. Alavi, E. N. Lay, and Z. A. Makhmali, "A CFD study of industrial double-cyclone in HDPE drying process," *Emerging Science Journal*, vol. 2, no. 1, pp. 31–38, 2018.

[36] S. Ghods, A. Kheyroddin, M. Nazeryan, and S. M. Mirtaheri, "Nonlinear behavior of connections in RCS frames with bracing and steel plate shear wall," *Steel and Composite Structures*, vol. 22, no. 4, pp. 915–935, 2016.

[37] R. Roshan, "Report of Kheirabad Dam Overflow Performance System," *Ministry of Water Research Institute*, WRI publisher, Iran, Tehran, 2019.

[38] M. R. Kavianpour, R. Roshan, and M. R. Najafi, "Controlling rooster tail development in gated tunnels," *International Journal on Hydropower & Dams*, vol. 20, no. 1, pp. 60–65, 2013.

[39] S. A. Hughes, "Physical models and laboratory techniques in coastal engineering," *World Scientific*, vol. 7, 1993.

[40] O. A. Yamini, S. H. Mousavi, and M. R. Kavianpour, "Experimental investigation of using geo-textile filter layer in articulated concrete block mattress revetment on coastal embankment," *Journal of Ocean Engineering and Marine Energy*, vol. 5, no. 2, pp. 119–133, 2019.

[41] O. A. Yamini, M. R. Kavianpour, and S. H. Mousavi, "Wave run-up and rundown on ACB Mats under granular and geotextile filters' condition," *Marine Georesources & Geotechnology*, vol. 36, no. 8, pp. 895–906, 2018.

[42] S.-R. Sabbagh-Yazdi and M. Bavandpour, "Numerical experiments on using incline collar rings for controlling mean and fluctuating forces on circular bridge piers," *Journal of Fluids and Structures*, vol. 91, Article ID 102696, 2019.

[43] M. Hambardzumyan and A. Hayrapetyan, "Differential diagnosis of malignant melanoma and benign cutaneous lesions by ultrasound analysis," *SciMedicine Journal*, vol. 2, no. 2, pp. 100–107, 2020.

[44] R. Reinauer and W. H. Hager, "Shockwave in air-water flows," *International Journal of Multiphase Flow*, vol. 22, no. 6, pp. 1255–1263, 1996.

[45] V. H. Vayghan, A. Saber, and S. Mortazavian, "Modification of classical horseshoe spillways: experimental study and design optimization," *Civil Engineering Journal*, vol. 5, no. 10, pp. 2093–2109, 2019.